Form-Finding with Isotropic Linear Weingarten Surfaces

Application to the design of membranes and funicular gridshells with planar quad faces

Xavier Tellier[1,*], Cyril Douthe[1], Laurent Hauswirth[2], Olivier Baverel[1]

[1] Laboratoire Navier, Ecole des Ponts, Univ. Gustave Eiffel, CNRS
77455 Champs-sur-Marne, France

[2] LAMA, Univ. Gustave Eiffel, CNRS

[*] Corresponding author e-mail: xavier.tellier@enpc.fr

Abstract

Isotropic Linear-Weingarten surfaces are a rich family of shapes, which contains some popular architectural surfaces such as paraboloids. We prove that these shapes are funicular for a uniform vertical load, and that the stress lines then form a conjugate net. This allows to design structures with planar facets, in which the edges have an optimal mechanical orientation. We introduce a generation method based on iterative projections. The method allows to intuitively control the shape by its boundaries and two design parameters. The formal potential is demonstrated on several examples.

Keywords: Architectural geometry, fabrication-aware design, funicular structures, gridshells, membranes, static equilibrium, structural design

1 Introduction

Curved envelopes allow for expressive architecture, and may offer impressive mechanical performances. The main challenge they induce is the geometrical complexity, which makes design, manufacturing and planning much more complex than with parallelepiped structures.

There exists many families of surfaces and associated generation methods to define the geometry of a curved object. Some particular families of surfaces combine mechanical and constructive properties, such as covering with planar quadrangles, and have natural intuitive generation methods. Popular examples include scale-trans surfaces, ruled surfaces, Monge surfaces, surfaces with planar curvature lines, developable surfaces, minimal and constant-mean curvature surfaces.

This article investigates a lesser known family of surfaces: isotropic Linear Weingarten surface, that we will nickname i-liwein surfaces for brevity. Examples are shown in **fig. 1**. This family turns out to have remarkable properties for application to architecture, and to have an intuitive shape behaviour.

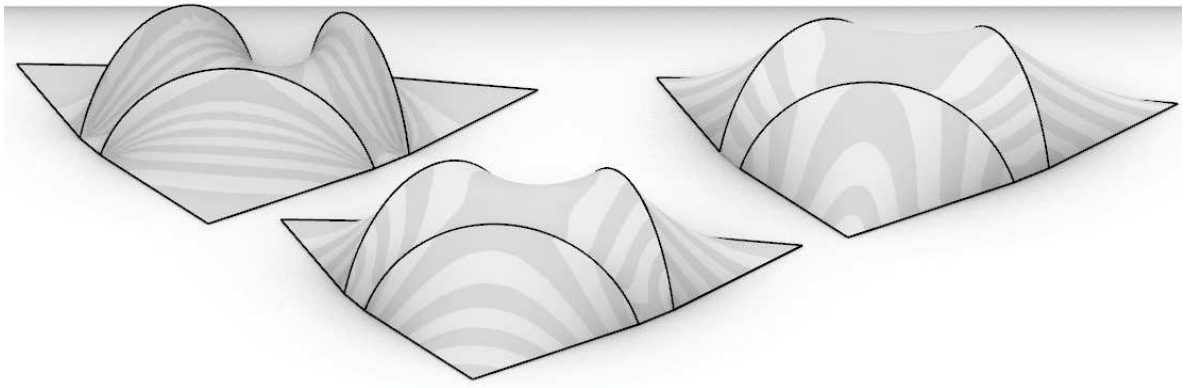

Figure 1: isotropic Linear Weingarten (i-liwein) tensile membranes generated on the same boundary curves (in black).

1.1 Overview of paper

In **sec. 2**, we introduce i-liwein surfaces. We first present basics of isotropic geometry, the context from which they emerge. In **sec. 3**, we show that i-liwein surfaces have an interesting mechanical property: they are funicular under a uniform vertical load, and the principal membrane stress directions then form a conjugate net. This makes them well-suited to design mechanically efficient support structures covered with planar quadrangles. We also show that a subset of i-liwein surfaces correspond to self-stressed membranes with, again, stress lines forming a conjugate net. In **sec. 4**, we show how they can be generated on target boundaries. The generation is equivalent to solving a Dirichlet problem of the Monge-Ampere

equation, and gives the user two degrees of freedom to control the shape. Finally, in sec. 5, we highlight some design applications to membranes, gridshells and funicular shells.

1.2 Previous work

The design of funicular surfaces under vertical loads has been well addressed by the literature (notably in Block 2009; Vouga et al. 2012). The question of combining funicularity with face planarity faces was also addressed by several authors. Schiftner and Balzer (2010) propose to draw maximum stress lines on a surface, and to then draw conjugate lines to obtain a quad grid, which can be optimized for planarity. Tang et al. (2014) propose a design approach based on the control of a coarse polygon and iterative subdivisions and optimization.

As principal curvature directions have many rationalization properties, Pellis and Pottmann (2018) propose to optimize a surface to align these directions with principal stress direction. A key to the method is to work with unstructured triangular mesh, and to then apply quad remeshing, an approach that will be used in this paper. Earlier work on that topic (Sun 2016) highlighted that fixing the mesh topology before the optimization is too constraining. Tellier et al. (2018, 2019) looked at the generation of constant mean curvature and Linear Weingarten surfaces (not *isotropic*), for which this alignment of stresses with curvature direction is obtained for a uniform normal pressure load.

2 i-liwein surfaces

2.1 Isotropic geometry

Isotropic Linear Weingarten surfaces are objects of *isotropic geometry*. Isotropic geometry is a way to describe the geometry of shapes with a specific set of tools, in which the vertical direction plays a particular role. A thorough treatment can be found in Sachs (1990). Pottmann and Liu (2007) gives a concise introduction.

In isotropic geometry, the notions of distance, angles and curvature differ from the traditional Euclidian geometry. They are all computed relatively to a vertical projection on the horizontal plane. The notion of surface curvature is also described differently. This difference is best understood by looking at a planar curve $z = f(x)$ (fig. 2). There are two ways to describe the inclination of the tangent of such a curve:

1. The angle it makes with a reference axis (e.g. a horizontal axis) ;
2. The slope dz/dx.

With the first one (the angle), the curvature is naturally understood as the variation of the angle of the tangent as we move along the curve ($d\alpha/ds$, with $ds = \sqrt{dx^2 + dz^2}$), which is the inverse of the radius of the tangent circle: this is the Euclidian curvature. With the second one (the slope), the curvature is best defined as the variation of slope with respect to x (d^2z/dx^2): this is the isotropic curvature.

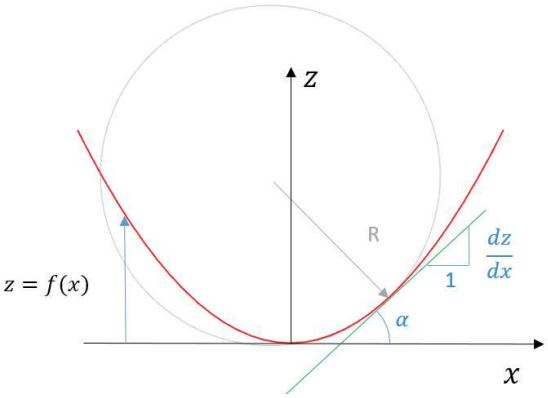

	Euclidian geometry	Isotropic geometry
Inclination	α	$\frac{dz}{dx}$
Curvature	$k = \frac{d\alpha}{ds} = \frac{1}{R}$	$k^i = \frac{d^2z}{dx^2}$

Figure 2: Description of curvature in Euclidian and isotropic geometry.

We remark that the slope of a vertical line is infinite: isotropic geometry is not the right tool to describe curves with vertical tangents or surfaces with vertical tangent planes. It is then natural to describe surfaces as field heights $(x, y) \mapsto (x, y, f(x, y))$. The role of the curvature tensor is played by the hessian of f:

$$\nabla^2 f = \begin{bmatrix} \partial_{xx} f & \partial_{xy} f \\ \partial_{xy} f & \partial_{yy} f \end{bmatrix}$$

$\nabla^2 f$ is symmetric, so it admits two orthogonal eigenvectors in the xy plane, which are called the *i-principal directions*. The maximum and minimum eigenvalues, $f_1$and f_2, are called *i-principal curvatures*. By integrating the i-principal directions on the surface, one obtains the i-principal curvature lines. They differ from the Euclidian principal curvature lines. However, they still form a conjugate net, which is a smooth equivalent of planar quad meshes (Sauer 1970). Furthermore, their vertical projection on the xy plane is an orthogonal net.

2.2 i-liwein surfaces

Similarly to Euclidian geometry, the Gauss and mean curvature can be defined as the determinant and half-trace of the curvature tensor (an *i* superscript is used to differentiate them from the traditional Euclidian curvatures):

$$K^i = \partial_{xx} f \partial_{yy} f - \partial_{xy} f^2 = f_1 f_2$$

$$H^i = \frac{1}{2}(\partial_{xx} f + \partial_{yy} f) = \frac{1}{2}\Delta f = \frac{1}{2}(f_1 + f_2)$$

i-liwein can then be defined as the surfaces verifying at each point:

$$aH^i + bK^i = c \tag{1}$$

for given constant real coefficients *a*, *b* and *c*. It turns out that some well-known families of surfaces fall into this category.

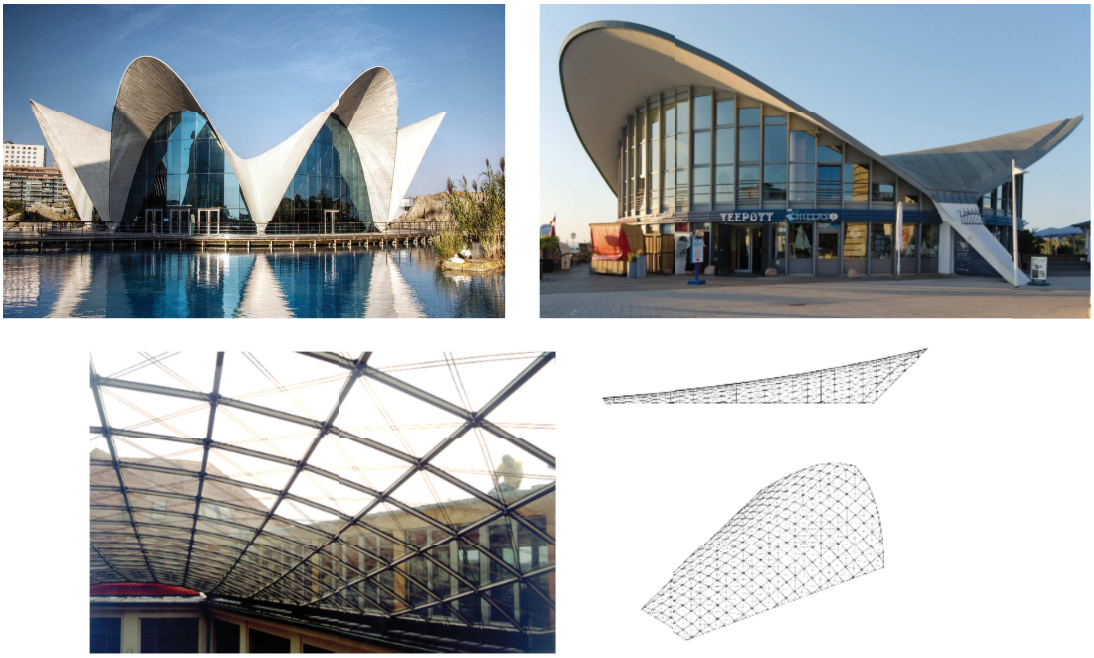

Figure 3: These three structure are composed of paraboloids, which are a special types of isotropic LW surfaces.Top left: El Oceanográfico (F. Candela), Valencia, Spain (©Felipe Gabaldón);Top right: Teepott restaurant, Warnemünde, Germany (©An-D) ;Bottom: Courtyard roof Industriepalast, Leipzig (reproduced with permission from Glymph et al. 2004).

Paraboloids

Paraboloids are a very common family of shapes for shells (see **fig. 3**). With a proper choice of axes and origin, their equation reads:

$$z{=}\alpha x^2{+}\beta y^2$$

If $\alpha\beta < 0$, the surface is called a hyperbolic paraboloid (or " hypar "), and contains two families of straight lines. If $\alpha\beta > 0$, the surface is called an elliptic paraboloid. The Hessian of the height field reads:

$$\nabla^2 f{=}\begin{bmatrix} 2\alpha & 0 \\ 0 & 2\beta \end{bmatrix}$$

Paraboloids are isotropic LW surfaces, as their mean and Gaussian curvature are both constant:

$$H^i = \alpha + \beta$$

$$K^i = 4\alpha\beta$$

There is actually one degree of freedom to define the (a, b, c) coefficients of the LW relationship (more precisely, one more degree of freedom than the trivial scaling of a, b and c). If we fix the trivial scaling of (a, b, c) by setting either $c = 0$ or $c = 1$, **eq. (1)** is verified for any value of a as long as:

$$b = \frac{c - a(\alpha + \beta)}{4\alpha\beta} \tag{2}$$

Pelikan surfaces

Membranes for which the membrane stress tensor, when projected in the horizontal plane, is constant, are called *Pelikan surfaces*. They were introduced in Pelikan (1958). These surfaces have been generated by dynamic relaxation (Hincz and Gaspar 1999) and have been used for example to design of membranes and concrete shells, such as the Keramion ceramics museum in Frechen (**fig. 4**), for which a tensile membrane was used as a formwork for a concrete shell (www.keramion.de).

Figure 4: The concrete shell of the Keramion museum in Frechen, Germany, is a Pelikan surface – a special type of i-liwein surface also referred to as i-minimal ©Klaas Vermaas.

Harmonic functions as height fields

Scalar harmonic functions of the plane are functions for which the Laplacian is null at any point: $\Delta f = 0$. They are therefore field heights of i-minimal surfaces, ie surfaces $H^i = 0$. There is a rich mathematical theory behind these surfaces. One method to generate a rich variety of analytical harmonic functions is via complex holomorphic functions (Cartan 1963). The link with i-minimal surfaces appears with an important theorem about holomorphic functions: Their real part and imaginary part are both harmonic.

Figure 5 shows several i-minimal surfaces generated using this property:

1. Top left: $f(z) = Re(logz\ )$ where $Re(z)$ is the real part of a complex number z.
2. Top middle: Monkey saddle of order 3: $f(z) = Re\left(z^3\right) = x^3 - 3xy^2$
3. Top right: $f(z) = Re\left(1/\|z\|^2\right)$
4. Bottom left: $f(x,y) = cosx\ exp(y-1) + cos(x+\pi)\ exp(-y-1)$
5. Bottom right: $f(z) = atan(z)$

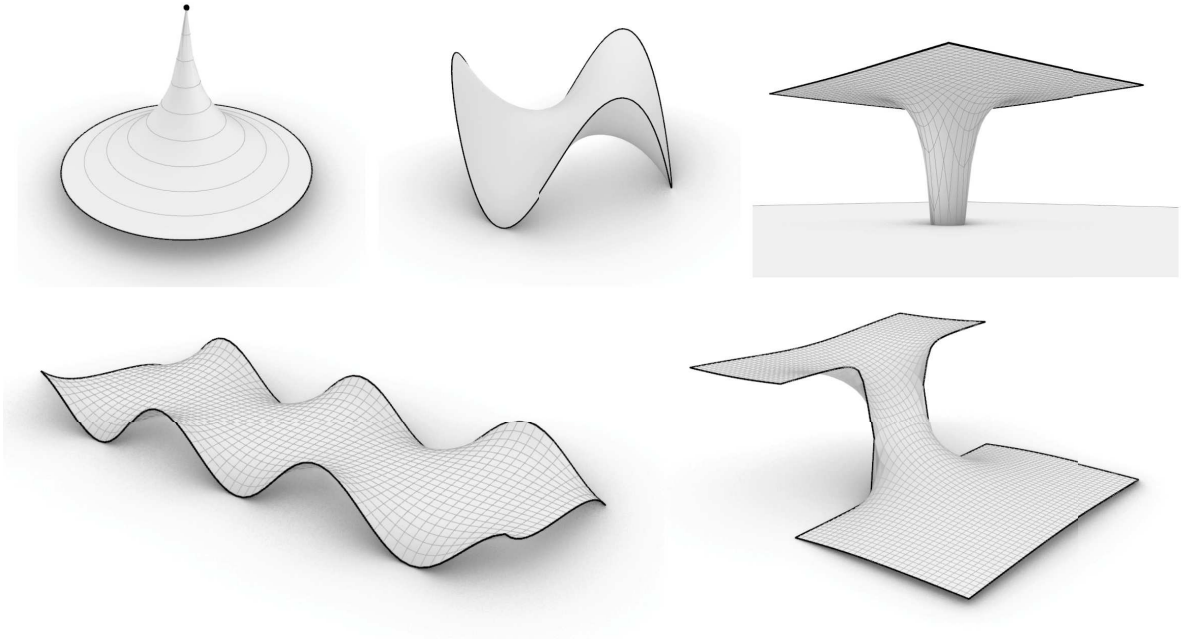

Figure 5: Analytical i-minimal surfaces – each surface can be realized as a tension membrane.

3 Mechanics of i-liwein surfaces

This section shows that i-liwein surfaces enjoy a mechanical property very similar to their Euclidian counterparts. This property is best expressed using the tensor N^i of projected membrane stresses in the xy plane.

Proposition

Let us consider a shell with membrane-compatible support conditions and with an i-liwein reference surface fulfilling **eq. (1)** ($aH^i + bK^i = c$). If $c \neq 0$, the shell is funicular for uniform vertical loads we_z (w in kN/m^2). The projected membrane stresses are given by:

$$N^i = \frac{w}{2c}\left(a\ I + b\ \widehat{\nabla^2 f}\right)$$

where I the identity tensor of the xy plane, and $\widehat{\nabla^2 f}$ is the tensor obtained by rotating the hessian $\nabla^2 f$ by $+90°$ around the z axis:

$$\widehat{\nabla^2 f}=\begin{bmatrix} \partial_{yy} f & -\partial_{xy} f \\ -\partial_{xy} f & \partial_{xx} f \end{bmatrix}$$

If $c=0$, the shell admits a one parameter family of self-stress fields given by:

$$N^i=\lambda\left(aI+b\widehat{\nabla^2 f}\right), \lambda \in R$$

Corollary

Under a uniform vertical load, principal membrane stresses on an i-liwein shell form a conjugate net. Discretization by stress lines hence give quadrangles which are near-planar.

Proof:

Membrane equations can be written in Cartesian coordinates, as detailed for example in Ventsel and Krauthammer (2001). The projected membrane stress field N^i is at equilibrium under a vertical load Ge_z if it verifies:

$$div\ N^i=0$$
$$div\left(N^i.\nabla f\right)=G$$

These equations correspond respectively to the horizontal and vertical equilibrium. The fact that $div\ N^i=0$ can be used to simplify the vertical equilibrium equation in the form:

$$tr\left(N^i.\nabla^2 f\right)=G$$

The divergence of the stress fields from the proposition are:

$$div\ N^i=\frac{w}{2c}\left(a\ div\ I+b\ div(\widehat{\nabla^2 f}\right)$$

Obviously, $div\ I=0$. Furthermore, by expressing $\widehat{\nabla^2 f}$ in x, y coordinates:

$$div\left(\widehat{\nabla^2 f}\right)=div\begin{bmatrix} \partial_{yy} f & -\partial_{xy} f \\ -\partial_{xy} f & \partial_{xx} f \end{bmatrix}=0$$

The proposed stress fields are therefore at horizontal equilibrium.

The vertical equilibrium is obtained by expressing $\nabla^2 f$ and $\widehat{\nabla^2 f}$ in the i-principal curvature directions. If $c\neq 0$:

$$
\begin{aligned}
tr\left(N^i.\nabla^2 f\right) &= \frac{w}{2c} tr\left(\left(a\begin{bmatrix}1&0\\0&1\end{bmatrix}+b\begin{bmatrix}f_2&0\\0&f_1\end{bmatrix}\right)\begin{bmatrix}f_1&0\\0&f_2\end{bmatrix}\right)\\
&= \frac{w}{2c}\left(a\left(f_1+f_2\right)+2bf_1f_2\right)\\
&= \frac{w}{2c}\left(2aH^i+2bK^i\right)\\
&= w
\end{aligned}
$$

The same reasoning applies to the case $c=0$. The corollary stems from the fact that eigenvectors of $\nabla^2 f$ are also eigenvectors of $\widehat{\nabla^2 f}$, which in turn are eigenvectors of $a\ I+b\widehat{\nabla^2 f}$.

Application to paraboloids

The above result can be applied to paraboloids with an interesting consequence: they are funicular for two different load cases. Given a paraboloid $z=\alpha x^2+\beta y^2$ we have two possible choices for parameter c, $c=0$ or $c=1$:

With $c=1$, we can interpret the shape as funicular under uniform vertical. Using **eq. (2)**, there is a one-parameter family of admissible stress fields:

$$
N^i=\frac{w}{2}\left(a\ I+b\ \widehat{\nabla^2 f}\right)=\frac{w}{2}\left(a\begin{bmatrix}1&0\\0&1\end{bmatrix}+\left(\frac{1-a\left(\alpha+\beta\right)}{4\alpha\beta}\right)\begin{bmatrix}2\beta&0\\0&2\alpha\end{bmatrix}\right)\ a\in R
$$

With $c=0$, we find another family of admissible stress fields, which corresponds to self-stressed states:

$$
\boldsymbol{N^i}=a\ \boldsymbol{I}+b\widehat{\nabla^2 f}=a\left(\begin{bmatrix}1&0\\0&1\end{bmatrix}-\frac{\left(\alpha+\beta\right)}{2\alpha\beta}\begin{bmatrix}\beta&0\\0&\alpha\end{bmatrix}\right),\ a\in R
$$

The fact that paraboloids are at the same time self-stress shapes and funicular shaped under uniform load is remarkable. For example, if a hypar membrane (case $\alpha\beta<0$) is used as a formwork for casting a concrete shell, the membrane deflection under the dead load of the fresh concrete is expected to be very low compared to other arbitrary membrane shapes: deflections will be mostly due to membrane stretching rather than to a deflection to get into a funicular shape. We remark that if $\alpha+\beta=H^i\neq\ 0$, warp and weft of the membranes need to be aligned with the horizontal x and y axes – otherwise the stress field is not admissible.

Invariance by x, y or z scaling

One can easily prove that the vertical scaling conserve the i-liwein property. However, a horizontal scaling (for example a 1D-scaling of x direction) transforms **eq. (1)**

into the form:

$$a_x \partial_{xx} f + a_y \partial_{yy} f + b_0 K^i = c_0$$

The same reasoning as above shows that these surfaces are also funicular under a uniform vertical load. In particular, scaling an i-CMC surface ($H^i = cte$) yields surfaces with constant projected stress tensors, i.e. a general Pelikan surfaces.

4 Generation of i-liwein surfaces from boundary curves

In this section, a generation method for elliptical i-liwein surfaces (verifying $a^2 + 4bc > 0$) from a boundary curves is presented. This part is rather technical, surfaces obtained with the proposed method will be shown in **sec. 5**.

4.1 The Monge-Ampere equation

As i-liwein surfaces are necessarily height fields, they can be generated by solving the EDP **eq. (1)** in a function f of z. This is a special case of the Monge-Ampère equation as it can be written in the form (Courant and Hilbert 1962):

$$E\left(\partial_{xx} f \partial_{yy} f - \partial_{xy} f^2\right) + A\ \partial_{xx} f + 2B\ \partial_{xy} f + C\ \partial_{yy} f + D = g(x,y)$$

With $E = b$; $A = C = \frac{a}{2}$; $B = 0$; $D = -c$; $g(x,y) = 0$

The Monge Ampere equation has many physical applications, ranging from optimal transport problems (Benamou et al. 2014; Villani 2003) to reflector design (Wu et al. 2013). It is also has applications in differential geometry, allowing for example the proof of the existence of particular types of surface (Trudinger and Wang 2008). Numerical resolution has been addressed quite recently by research. A review of is given in Neilan et al. (2020).

This equation is particularly complex to solve for the following reasons:

1. It is a fully nonlinear problem : The term with highest derivative is not linear;
2. Solutions have low regularity and are not unique;
3. Weak solutions are not based on variational principles. A significant portion of the literature is devoted to viscosity solutions, which may have weaker regularity;
4. Existence and uniqueness of solutions is subject to a constraint on the convexity of the solution and domain – which is a strong constraint for application to architecture.

Many resolution methods are based on finite differences and a quad grid discretisation of the plane (Dean and Glowinski 2003; Oberman 2008; Benamou et al. 2010). These are less suited for irregular contours, as are likely to occur in an architectural context. Also, these methods only search for a convex solution to the problem, which we will refer to as *type II*, in **sec. 4.3**.

Feng and Jensen (2017) introduced a finite-element formulation based on a triangular discretization. It was used in Jensen (2018) to explore some solutions of the Monge-Ampere equation on non-convex domains. As this method is relatively complex, we will use the fact that, in our context, $g = cte$, to propose a simpler generation method based on a quadratic discrete operator from discrete differential geometry.

4.2 Discrete i-liwein surfaces

We use the vertex-wise discrete model for H^i and K^i for unstructured triangular meshes proposed in Pottmann and Liu (2007). From these discrete models, *i-liwein triangular meshes* can naturally be defined as meshes for which a linear combination of these two curvatures is constant for each vertex:

$$\forall\ vertex\ v,\ \ aH^i(v)+bK^i(v)=c,\ \ a,b,c\in R$$

4.3 Preliminaries on smooth i-liwein surfaces

Type I and II solutions

Important geometrical insight can be obtained from the curvature diagram, i.e. a diagram plotting the value of H and K at each surface point (**fig. 6**). For i-liwein surfaces, this diagram is included in a straight line. We observe that the isotropic Gaussian and mean curvature verify the inequality:

$$H^{i\,2}-K^i=\left(\frac{f_1-f_2}{2}\right)^2\geq 0$$

There is hence a domain of the diagram which is impossible geometrically (in red). If $a^2+4bc\geq 0$, the line defined by **eq. (1)** crosses this forbidden domain. The curvature diagram is hence included in the union of two rays (semi-infinite lines). Now, in a smooth surface, curvatures vary continuously: the curvature diagram is one connected domain. As a result, the curvature diagram of an i-liwein surface with $a^2+4bc\geq 0$ cannot be on both rays. We will call type I (resp. type II) the i-liwein surfaces having their curvature diagram entirely in the left (resp. right) ray.

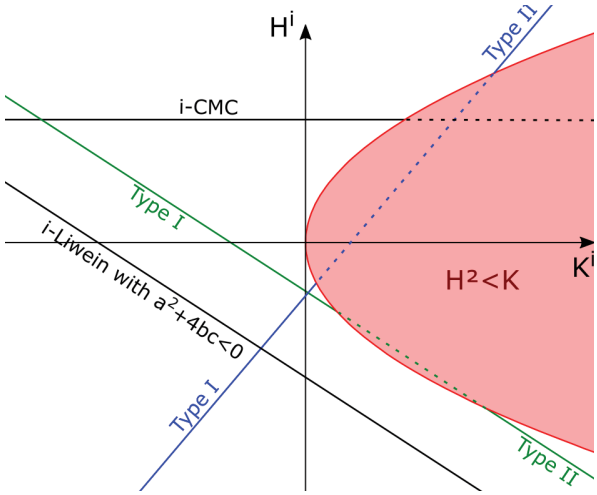

Figure 6: Curvature diagram.

Condition for elliptic PDE

One can show that, if $b \neq 0$, **eq. (1)** can be put in the following form with the change of variable $g(x,y) = f(x,y) + \frac{a}{4b}(x^2+y^2)$:

$$4b^2 K^i(g) = a^2 + 4bc$$

Solving **eq. (1)** with $a^2+4bc>0$ is therefore equivalent to computing the geometry of a surface with positive constant i-Gaussian curvature. This problem is elliptic, and is hence well suited to a generation from a closed boundary.

4.4 Generation method

Iterative resolution

We introduce an iterative method to solve the equation, with the following simple pseudo-code:

- *Triangulate domain*
- *Create initial solution (e.g. z=0 or minimal)*
- *Iterate until displacements are below tolerance:*
  - *Solve the equation aHi+bKi=c for each vertex individually, assuming that neighbours are fixed.*
  - *Move each vertex to the calculated position.*

Local resolution

The key step of the algorithm is the resolution with fixed neighbours. The equation is non-linear. However, we remark that, as the center vertex of a 1-star is moved

along a vertical axis, the models for H^i and K^i vary respectively linearly and quadratically. Therefore, $aH^i + BK^i - c$ is quadratic in z. Hence, there exists real coefficients α, β and γ such that:

$$aH^i + bK^i - c = P(z) = \alpha z^2 + \beta z + \gamma$$

The resolution in z is then straightforward. As there are two solutions, we choose the one with lowest K^i to obtain a type I solution. If $a^2 + 4bc$, is negative or near zero, we observe numerically that there is no solution to this quadratic equation. Future work could address finding a discrete equivalent of the condition $a^2 + 4bc > 0$ for elliptic i-liwein surfaces.

Discussion

Despite the lack of theoretical results on the existence of solutions, it was found to work satisfyingly well. The quality of the resulting meshes was validated by measuring the convergence to paraboloids.

The main limitation is for non-convex boundaries, for which the existence of solutions is not guaranteed. If parameter b is pushed to a value for which there is no solution to the Dirichlet problem, the vertex height diverges. This may happen even at low values of b if the domain has holes with a highly curved boundary.

The generation of shapes of **fig. 7** to **9** and **11** takes about 15s on a 2.0GHz single-core processor with 8MB RAM, with initialization from a planar mesh. The user can visualize the shape being deformed at each iteration, such that a good idea of the final shape can be obtained within 5-10s, and parameters can be adjusted at any time, in the same way as in a software like Kangaroo2.

The current method does not allow for funicular boundaries, like for example a membrane held by cables. Future work could address this problem by treating boundary vertices with dynamic relaxation, as was recently done for Euclidian Linear Weingarten surfaces in Tellier et al. (2020).

Regarding numerical performance, the current algorithm moves vertices one-by-one. It could be made much faster using Newton like finite-difference schemes. In particular, if $b = 0$, our algorithm does not benefit from the linearity of the problem. Faster resolution methods are a topic of future work.

5 Designing with i-liwein surfaces

5.1 Membranes

With $c = 0$, surfaces $aH^i + bK^i = 0$ correspond to the equilibrium shapes of self-stressed membranes. The shape of i-liwein membranes can be understood by comparing i-minimal with minimal surfaces. Compared with minimal surfaces, i-minimal surfaces:

1. Do no not have uniform stresses. Their projected stresses are uniform, which implies that the membrane stresses are higher in areas of high slope (and theoretically infinite if the surface has a vertical slope);
2. Are restricted to shapes that are field heights;
3. Can join boundaries with significant height difference, which cannot be interpolated by a single minimal surface.

The shape differences are illustrated in **fig. 7**. i-minimal and minimal surfaces are created on the same three boundaries, with increasing height differences between the large oval on the ground and the two loops at the center. In the top row, the height difference is quite low, such that the difference between the two surfaces is hardly noticeable. In the middle row, the height difference is increased: the difference between the two surfaces is clear. Necking is observed in the minimal surface around the center loops, but not for the i-minimal surface, which is actually just a scaled copy (in the z-direction) of the one above. In the bottom row, the height difference is further increased. There does not exist anymore a stable minimal surface fitting the boundary curves.

i-liwein membranes do not require that the isotropic direction is vertical: whatever the direction, they correspond to a self-stressed membrane geometry. Therefore, on a given boundary, the isotropic direction can be tilted to explore shape variations. An example is shown in **fig. 8**, where three i-minimal surfaces are generated on the same boundaries (two coaxial circles), but with different isotropic directions (indicated by red arrows). In each case, the stresses projected in the plane perpendicular to the red arrows are constant. The effect of parameter b on the geometry can be visualised in **fig. 1**. It makes the surface tend towards the upper or lower portion of the convex envelope of the boundary curves.

Figure 9 shows shows Pelikan surfaces obtained by scaling the boundary in the x or y direction of an i-minimal surface (middle), creating an i-minimal surface on it, and scaling everything back to the original boundary. This result in with increased transverse (left figure) and longitudinal (right) tension.

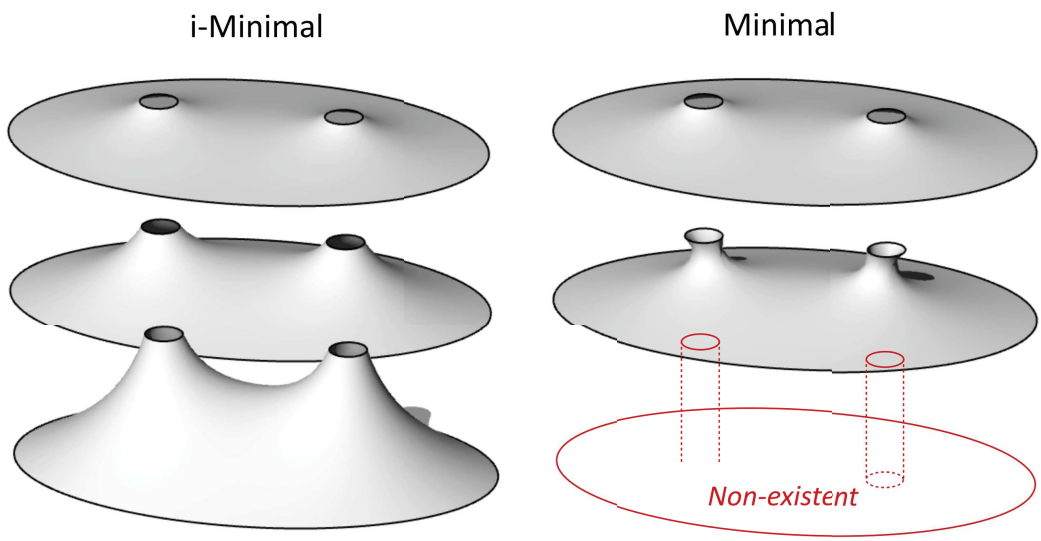

Figure 7: Comparison of the shape of i-minimal and minimal membranes on three sets of boundary curves, with increasing height difference.

Figure 8: i-minimal membranes constructed on the same boundary, but with different isotropic directions.

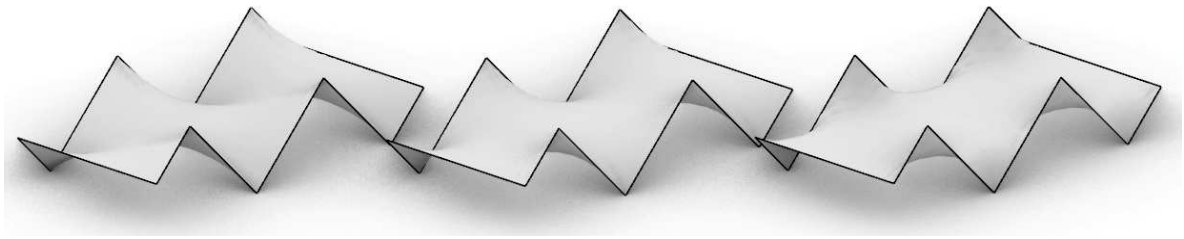

Figure 9: Middle: i-Minimal surface. Left and right: Pelikan surfaces with respectively increased transverse and longitudinal tension.

5.2 Gridshells

For a gridshell, i-principal curvature directions of i-liwein surfaces have both fabrication and mechanical properties. An application is illustrated in **fig. 10**. An i-CMC surface is generated on a boundary composed of four closed curves. An i-principal curvature net is computed, and is used to define the position and orientation of the beams of a gridshell. Since the i-principal net forms a conjugate curve network, mesh faces are almost planar (an optimization could make them planar with small vertex displacements). Furthermore, beams are aligned with principal stress directions under uniform vertical pressure (snow load), so they have a relevant orientation. Finally, we can notice that pattern drawn by i-curvature lines is smooth, and gives faces with approximately uniform size.

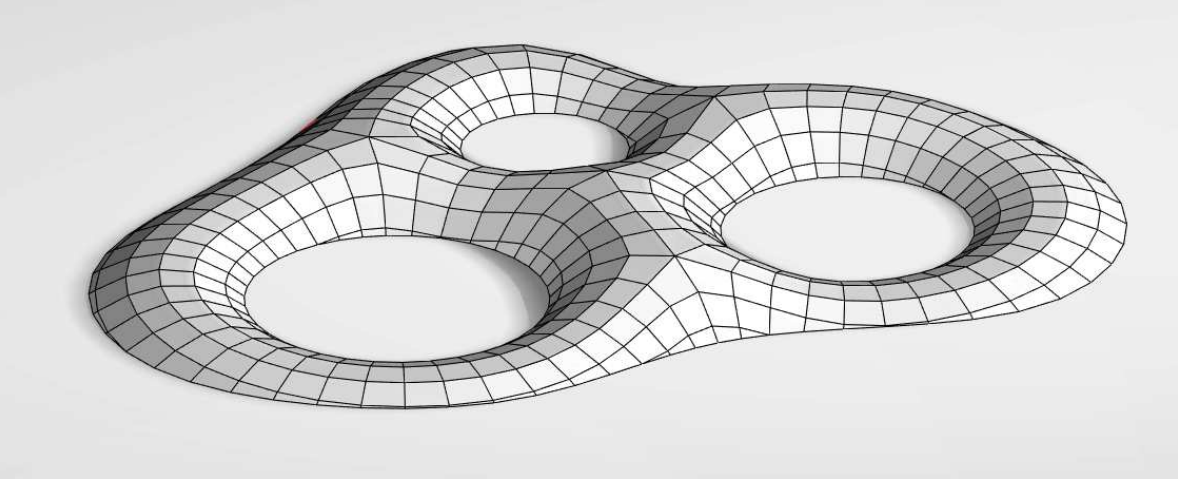

Figure 10: Funicular gridshell with planar quads, constructed by discretizing an i-CMC surface along i-principal curvature directions.

If one were to search by optimization of vertex positions the geometry of a gridshell combining planar quads and beams aligned with principal stresses, a main question would be: what is the right mesh combinatorics to start with? In i-liwein surfaces, this combinatorics appears naturally from the curvature field.

Regarding structural behaviour, i-liwein gridshells are funicular for a uniform vertical load, provided that lateral forces can be resisted at the supports. A uniform vertical load is a good approximation of selfweight if the envelope slope remains low, and it also corresponds to a uniform snow load. Asymetric load cases and buckling would also need to be considered for a gridshell design. Eventhough i-liwein surfaces might not be optimal for these, they still form a rich and efficient design space for conceptual design phases.

5.3 Funicular shells

i-liwein surfaces can also be used to design funicular shells. The method allows a quick exploration of a 2-parameter family of funicular surfaces fitting a target boundary. For a concrete shell, the fact that i-principal curvature lines form a conjugate net could be used to simplify the fabrication of formwork. For example, the surface can be covered with developable strips so that thin flexible panels can be used as formwork.

The effect of parameters b and c on the surface geometry are the following: parameter c allows to more or less inflate the surface (with a pressure acting vertically), while parameter b allows the control of the height difference between saddles and hill tops. This is illustrated in **fig. 11**, in which the reference surface of **fig. 10** (which is i-CMC) is deformed. The left picture shows the case $b<0$: the surface looks like domes connected by low corridors. The right picture shows the case $b>0$: the surface now looks level, a more unified space is defined underneath.

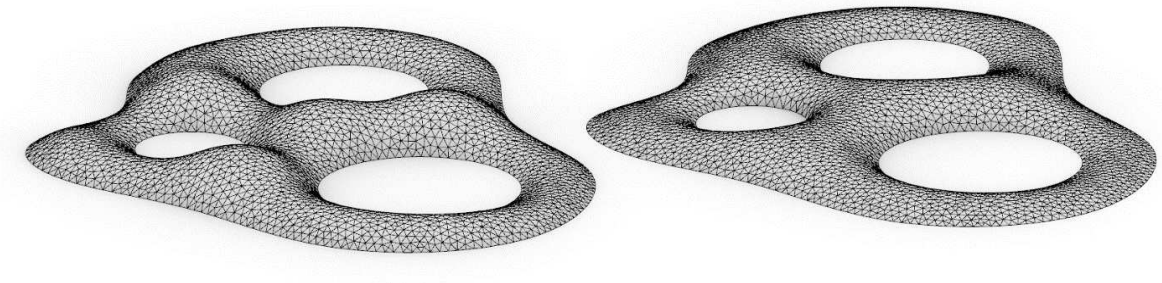

Figure 11: i-liwein surfaces generated on the same boundaries as the gridshell of **fig. 10**. Left: b>0. Right: b<0, close to the limit $a^2 + 4bc = 0$.

6 Conclusion

This article showed the relevance of isotropic Linear Weingarten for architectural design, with applications to popular structural systems. It was proven that they are funicular for a uniform vertical load, and a generation method was proposed. i-liwein surfaces appear to offer an interesting design space, with a control from boundary curves which is well suited for many architectural projects. Parameters a, b and c offer a global shape control, which is particularly interesting for editing complex shapes. The low amount of preprocessing required for the designer makes this method particularly suited in the context of conceptual design explorations. On a final note, it is remarkable to observe how Linear Weingarten surfaces are funicular for a normal pressure or a vertical pressure depending on the type of geometry used to define the curvature, Euclidian or isotropic.

Acknowledgement

We would like to warmly thank Pr. István Sajtos for bringing Pelikan surfaces to our attention, as it initiated this project on isotropic linear Weingarten surfaces. We would also like to warmly thank Laurent Monasse for fruitful discussions.

References

Benamou, J. D., B. D. Froese, and A. M. Oberman (2010). Two numerical methods for the elliptic Monge-Ampère equation. *ESAIM: Mathematical Modelling and Numerical Analysis 44*(4), 737–758.

Benamou, J.-D., B. D. Froese, and A. M. Oberman (2014). Numerical solution of the Optimal Transportation problem using the Monge – Ampère equation. *Journal of Computational Physics 260*, 107–126.

Block, P. (2009). *Thrust Network Analysis. Exploring Three-dimensional Equilibrium*. Ph. D. thesis, MIT.

Cartan, H. (1963). *Elementary Theory of Analytic Functions of One or Several Complex Variables* (Editions s ed.). Addison-Wesley Inc.

Courant, R. and D. Hilbert (1962). *Methods of mathematical physics - Volume II - Partial Differential Equations*. Wiley-VCH Verlag.

Dean, E. J. and R. Glowinski (2003). Numerical solution of the two-dimensional elliptic Monge-Ampère equation with Dirichlet boundary conditions: An augmented Lagrangian approach. *Comptes Rendus Mathematique 336*(9), 779–784.

Feng, X. and M. Jensen (2017). Convergent semi-lagrangian methods for the monge–ampere equation on unstructured grids. *SIAM J. NUMER. ANAL 55*(2), 691–712.

Glymph, J., D. Shelden, C. Ceccato, J. Mussel, and H. Schober (2004). A Parametric Strategy for Freeform Glass Structures Using Quadrilateral Planar Facets. *Automation in Construction 13*(2), 187–202.

Hincz, K. and Z. Gaspar (1999). The effect of the apporximations used during generation of membrane cutting pattern.pdf. *Archives of Civil Engineering 45*(2), 221–230.

Jensen, M. (2018). Numerical Solution Of The Simple Monge–Ampère Equation With Nonconvex Dirichlet Data On Nonconvex Domains. In

Hamilton-Jacobi-Bellman Equations, pp. 129–142. Walter de Gruyter GmbH,Berlin/Munich/Boston.

Neilan, M., A. J. Salgado, and W. Zhang (2020). The Monge–Ampère equation. In *Handbook of Numerical Analysis*, pp. 105–219.

Oberman, A. M. (2008). Wide stencil finite difference schemes for the elliptic Monge-Ampère equation and functions of the eigenvalues of the Hessian. *Discrete Contin. Dyn. Syst. Ser. B, 10*(1), 221–238.

Pelikan, J. (1958). Membrane structures. In A.-J. A. and E. Al. (Eds.), *Proc of the Second Symp. on Concrete Shell Roof Construction, Teknisk Ukeblan, Oslo*.

Pellis, D. and H. Pottmann (2018). Aligning principal stress and curvature directions. In *Advances in Architectural Geometry*, Number September, pp. 34–53.

Pottmann, H. and Y. Liu (2007). Discrete Surfaces in Isotropic Geometry. *Methods* (i), 341–363.

Sachs, H. (1990). *Isotrope Geometrie des Raumes* (Vieweg ed.).

Sauer, R. (1970). *Differenzengeometrie*. Springer, Berlin.

Schiftner, A. and J. Balzer (2010). Statics-Sensitive Layout of Planar Quadrilateral Meshes. In *Advances in Architectural Geometry*, pp. 221–236.

Sun, X. (2016). *Discrete Curvature Theories and Applications*. Ph. D. thesis, Ph. D. thesis, King Abdullah University of Science and Technology, Thuwal.

Tang, C., X. Sun, A. Gomes, J. Wallner, and H. Pottmann (2014). Form-finding with Polyhedral Meshes Made Simple. *Transactions on Graphics 33*(4).

Tellier, X., C. Douthe, L. Hauswirth, and O. Baverel (2019). Linear Weingarten surfaces for conceptual design. *Proceedings of the International fib Symposium on Conceptual Design of Structures*, 225–232.

Tellier, X., C. Douthe, L. Hauswirth, and O. Baverel (2020). Linear-Weingarten membranes with funicular boundaries. *Structural Concrete*, 1–14.

Tellier, X., L. Hauswirth, C. Douthe, and O. Baverel (2018). Discrete CMC surfaces for doubly-curved building envelopes. In *Advances in Architectural Geometry*, pp. 166–193.

Trudinger, N. S. and X.-j. Wang (2008). The Monge-Ampère equation and its geometric applications. *Handbook of Geometric Analysis, International Press I*, 467–524.

Ventsel, E. and T. Krauthammer (2001). *Thin Plates and Shells. Theory, Analysis and Applications*, Volume 66. Marcel Dekker.

Villani, C. (2003). *Topics in Optimal Transportation*. American Mathematical Society.

Vouga, E., H. Mathias, J. Wallner, and H. Pottmann (2012). Design of Self-supporting Surfaces. *ACM Trans. Graph. 31*(4).

Wu, R., L. Xu, P. Liu, Y. Zhang, Z. Zheng, H. Li, and X. Liu (2013). Freeform illumination design : a nonlinear boundary problem for the elliptic Monge – Ampére equation. *Optics Letters January*, 229–231.